Journal of Solar Energy Research (JSER)

Journal homepage: www.jser.ut.ac.ir

Porous Jump Model to Interpret the Effect of Perforated Absorber Layer Inclination On Solar Cooker Reliability

Suhaib J. Shbailat[a*], Israa R. Jawad[b], Jenan S. Sherza[c], Ahmed F. Khudheyer[d]

[a,b,d] *Mechanical Engineering Department, College of Engineering, Al-Nahrain University, Baghdad, Iraq*
[c] *Department of Mechanical Engineering, University of Technology, Baghdad, Iraq*

ARTICLE INFO

Article Type:

Research Article

Received:24.05.2024
Accepted:07.11.2024

Keywords:
Box-type solar cooker,
Perforated Plate,
Absorber incline angle,
Cooking power,
Cooking time

A B S T R A C T

Energy is one of the many problems concerning the future of sustainable development since it is limited in quantities. Investments should be re-employed and new technologies should be employed. The use of solar stoves will be one possible approach. In numerical tests of box-shaped solar cookers, the heat absorber plate was copper perforated, and we examined the heat absorption levels for inclined angles of 0°, 3°, 6°, and 9°. The research revealed that the perforated copper lid of the cube-based facade of the solar cooker reached a level of almost 18.4 degrees higher than the regular absorber. Moreover, the cooking time in the box-shaped solar oven will shorten by 21% when the manufacturer uses a perforated copper plate instead of a regular flat one in production. In the first test, the best internal air temperature was obtained by an inclination of 9 degrees. Consequently, the mean temperatures of the perforated copper absorber plate were raised with increasing inclination angles. In this case, the equation for cooking power demonstrated how the cooker steadily heated up and used water in the right range throughout the selected period.

1. Introduction

A lot of the yearly energy consumption is brought about by energy involved in cooking, although it is only one of several other energy consumptions. Such appliances can be sources of clean power if a properly made solar-powered kitchen tool is available. Nevertheless, using gas and electric equipment in kitchens has become very popular, while old fuels such as coal, kerosene, wood, animal manure cakes, and all types of agricultural residues remain in use. According to the World Energy Statistics (2017) [1], the consumption of energy in residential and commercial sectors comes up to 30% or more of the total energy commodity use worldwide. The rate will differ if the area's culture is social and the geography is taken into consideration. The only way to plan for the energy of the forthcoming years is sustainable technologies that use non-conventional resources now, so they are vital. On

*Corresponding Author Email: suhaib.j.shbailat@nahrainuniv.edu.iq

Cite this article: Alshbailat, S., Jawad, I., Sherza, J., & Khudheyer, A. (2024). Porous Jump Model to Interpret the Effect of Perforated Absorber Layer Inclination on Solar Cooker Reliability. Journal of Solar Energy Research, 9(3), 2010-2024. doi: 10.22059/jser.2024.376901.1417

DOI: 10.22059/jser.2024.376901.1417

the other hand, it cannot be overstated that solar energy-based systems (SEBSs) are in demand. Consequently, solar cookers shall act as a vital factor in solving today's energy disaster [2].

A straightforward option is the solar cooker. This cooker does not need fuel or coal, saving time spent cutting trees. The application of solar ovens can empower women to save time and reduce their environmental influence. Making use of solar cookers, they cooked food for their families, allowing them to save firewood and reduce exposure to smoke. The most typical types of solar cookers are photovoltaic box cookers, parabolic cookers, and panel cookers [3]. In the framework of the solar cooker (enclosure), solar radiation is converted together into thermal energy, which in turn increases the temperature. The heat-insulated smokeless stove also gives out considerable heat and can house several pots. The next type of solar cooker is parabolic, focusing the sun's rays to heat up gradually. On the other hand, this preheater is somewhat challenging to use because it requires ongoing observation and fine-tuning. The next form is a solar cooker of different sizes. The panel solar cookers have a box and a concentrator absorber set advantages [4]. The low production cost and simple usage of this solar cooker have resulted in its wide acceptance among the masses. Designing a highly efficient solar cooker is a complicated task as many factors should go into such a device. The end-user experience is advanced through a redesign of the solar cooker absorber plate that has been done by the researchers [5]. We will not be in a position to fully consider the fact that using the ineffective energy of the solar box cookers consumes much time in cooking. In Iraq, the use of solar cookers lost popularity, and the country didn’t embrace it as much as other countries. To ensure the solar cooker's coverage, a new absorber plate design is needed.

Solar cookers suffer from the problem of convection because air, as a primary property of the convection, has poor thermal capacity and heat transfer coefficient. Moreover, the efficiency of this solar cooker is reduced slowly because about 55% of the energy from the sun is lost during the time that the rays hit the cooker [6]. Due to having a lower heat transmission coefficient, air solar cookers are not regarded as being very efficient. This is done by enhancing the value of the heat transfer coefficient on the top plate of the absorber with an artificial roughness [7]. The precedent studies utilized highly efficient methods of dropping the heat loss of the solar cooker by using a long hood and insulation. Fins can promote heat transfer, while the phase change material (PCM) may grant the extension of ventilation cycle duration. Moreover, the perforated plate is a porous material that is set in the flow way of a solar cooker as an absorber plate. As a passive technique of heat transfer, it is an approach with high heat gain [8].

In addition to heat transfer and carrying thermal qualities, the perforated plate can be used as a pattern for fluid flow when it is put in a solar cooker. The size and range of interactions of the burning perforated plate can be realized by pre-shaping and fitting the perforated plate into the solar cooker at different angles. Fluid disruption is the process of disrupting the flow pattern, which results in heat dissipation across the entire region. The drainage of the solar cooker can be made to advantage just as well the perforated plate structure's tiny pores, its poor permeability and its potential to be an effective parabolic and instructor [9].

The paper novelty focuses on the effectiveness of solar cookers and the visual numerical of a prototype sun cooker that uses a normal temperature absorber and a perforated plate with an independent sun cooker in a closed system. In the following work, an emphasis will be on the absorber plates' efficiency formed by the perforated sheet, and quantitative data on how this would affect the solar cooker's performance will be presented.

2. Literature review

To achieve the objective of improving box-type solar cookers, below are some of the methods that have been written by researchers in different kinds of literature. Ashby et al. [10] presented their research on solar cookers box-type and found the results of their research useful to others planning to do the same. They were not only been able to provide simulations showing the solar cooker as a box-type, but they have also been able to obtain the maximum elevation for the house to determine the behaviour of the absorbent and the pot, as well as take into account the effect of conductivity of the absorbent. Tan et al. [11] studied A multi-reflector box solar cooker with some interior reflectors of several stages. It has been studied using a second law approach. The thermodynamic efficiency of the given category of devices was presented based on the explanation of the second law. The construction costs and 5% production figures under these cooker's temporary conditions after a few hours of operation make it possible to talk seriously about this type of solar cooker. J. Nayak et al.[12], offered a preliminary mathematical model for a box-type solar cooker,

whose top is hinged but with only a frontal reflector. This problem uses an analytical method of solving the main cooker elements' circuit, which can be easily done using Cramer's rule. It is commonly believed that many heat transfer coefficients change with a certain temperature level. A. Ukey et al. [13] concentrated on analytical approaches to express temperatures in various zones of one cooker when another one was tested in Tanta, Egypt. With their observation, they inferred diverse thermal phenomena. For the box-type solar cooker with outer-inner reflectors, M. Noman et al. [14] provided a simple mathematical model, the analytical solutions of energy-balanced equations that give each cooker element its basis. Through the computer simulation, we research the cooker's efficiency, boiling characteristics, and specific boiling times. Hashemian and Noorpoor [15] presented a new design of a multi-generation system to utilize both biomass and solar energy for the production of electricity, heat, coolness, hydrogen and drinking water. The system consists of a steam Rankine cycle, a double effect absorption chiller, a proton exchange membrane electrolyzer, multi-effect desalination as well as the parabolic trough solar collector. A thermodynamic analysis is performed to illustrate the thermodynamic performance and failure by determining the loss of work in the components. Exergoeconomic analysis provides product cost rate of different products and cost flow in the investigated system. Further for this purpose along with the exergy analysis to evaluate the amount of environmental effect of the suggested system the exergy environmental analysis is carried out and described. The findings of the work show that the feasible enhancement of energy efficiency, exergy efficiency, total product cost rate and exergy environmental impact of the multi-generation system are 82.4%, 14%, 0.84 $/s and 0.15 respectively. From the Pareto frontier, a design scheme corresponding to the exergy efficiency of 16.53% and the product cost rate of 0.71 $/s is chosen as the best design. In a separate work, G. G. Engoor et al. [16] established a mathematical model of a solar box cooker and concluded that a large number of parameters are involved in the thermal performance of these cookers. Moreover, it sets up a parametric model of the solar cooker's operation, which can provide information on the power it will cook with. Thus, heatstroke, temperature difference, and load distribution were the three uncontrolled factors for the model, while the area of the solar interception, the overall heat loss coefficient, and the thermal conductivity of the base were the three controlled variables. This model, the solar commercial cooker, was used as part of the validation. As the rectangular solar cooker performance is to be forecasted, E. Vengadesan and R. Senthil [17] developed a straightforward way to determine the design parameters. To calculate two figures of merit, index F_1 and coefficient F_2, an extra series of experiments was done on a double-glazed solar cooker that has an aperture area of 0.24 m^2. Hence, the next step after calculating the heating curves is to employ the suggested approach for the different dosages of water. Based on the result of the box-type solar cooker presented by Singh [18], the effectiveness of having inside reflector walls was assessed in two different setups. The first one was an out-of-ordinary test for a long time (10 h), while the second one was to compare it with a work previously made in Tanta, Egypt. For the numerical part, the authors applied finite differences in water baths. The water was left to boil or reach its maximum temperature by using the hot storage block as a resting ground for the pot. Time was the next calculation. I built the casting box of cast iron and granite rocks (stone) and then conducted numerical calculations for the pot size. Thermal measurements were conducted in the sunlight layer for different diameters of the flower head to the stem. In recent years, Tawfik et al. [19] coupled the explanations of the factors such as the distance and angle of the solar box cookers can be operated. 202°C was the cooking temperature achieved by the top solar cookers for them on October 7, 1997, between 12:00 and 12:45 p.m. This cooker can thus be used for a long time because it can store heat for a very long time and be utilized later on. A new design, HS 5521, HS 5521, which was thought to be the best version in terms of size, reflector area, insulator thickness, oven volume, and aperture area, was introduced after optimizing them. It cost less to make the second model than the first one, and the market volume was only 35% of the referee model. Saxena et al. [20] created a complicated math model that considers heat conductivity in a solar cooker, a type of box that contains foods. Daylight and a dish/vessel placed on top of the bottle will also be considered. Different length bind intervals were assessed. Then, a simulator is applied to evaluate each of the air temperature, food temperature, the one for the top cover, and the internal wall on all sides. The entire cooking procedure was accompanied by solar radiation, which was considered in the provided results. We exhibited some results from the tests of the Sonnenblum samples. He then went on to proceed with his demo, where he went through all the basics of food, including weather resistance, the thermal resistance of box walls, and any adjustments to the box while cooking all the food to get the accurate

temperature. To establish the efficiency of a solar cooker, consisting of a box-type type, Sagade et al. [21] suggested that two heat transfer models should be employed: the models for the sun irradiance and the ambient temperature. The two transport mechanisms, namely convection and conduction, would ultimately be the subject of the model. A year-long comparison between rates of solar cooker efficiency was used in various countries to make the design of solar cookers. After the end of one month of recording the temperatures; the modelling was found to have an absolute error of less than 4%, confirming that could be used to make accurate predictions. The convective heat flux coefficients in our model were determined through the use of experimental temperatures measured at different points of the solar cooker. Values of 2 W/m² K for the indoor air to absorbent plate coefficient, 3 W/m² K convection between the air in the cooker and the interior wall surfaces, and 4.5 W/m² K convection between the exterior wall surfaces and the atmosphere were measured. Ruivo et al. [22] conducted a computer analysis to determine how much heat loss would occur from the use of a trapezoidal-shaped solar cooker, considering the influence of radiation and natural convection. The software that was used to run the mortgages was FLUENT 16.0. The steady compressible flow of heat transfer through a film has experimented and radiation boundary conditions, temperature, and film coefficient were used. The flow direction of the cavity and isotherms (isolines) were determined using different criteria applied. With about 70-80% of the heat loss caused through the radiation heat loss from the cavity, which is a major part of the total heat loss, experimental correlations obtained between the temperatures averaged Nusselt number and its influence factors of the solar cooker cavity have been extensively used. Aquilanti et al. [23] stated that while inspecting weather data in Quetta, Pakistan, researchers identified thermal factors that were unique to a cooker box-type solar cooker. Both ASAE S580: The recommendation of using F_1 and F_2 testing, standard cooking power, efficiency, and cooking power testing was given by ISO 13429:2000 in 2003 and BIS IS13429:2000. The thermal efficiency was tooled to assess the solar cooker by running the heater for five consecutive sessions. Through calculations the values of F_1 and F_2 were assessed, F_1 equalled to 0.12 and F_2 equalled to 0.58 the average thermal performance was constructed for the five-day experiment and it was 29.81%. The results ranged within the values accepted and provided by test conditions. A closed sun cooker with 12 copper segments for TES was built and evaluated by Aquilanti et al. [24]. Paraffin wax, granulated charcoal powder, and a certain combination of the two TES materials made testing the cooker's performance possible. The measured efficiency was increased by 53.81%, the heat loss coefficient at the process global scale was minimized to 5.11 W/m² °C, the cooking power was calculated to be 68.81 W, and the heat transfer coefficient was determined to be more effective at 56.78 W/m² °C. There is a solar cooker called a Quonset Cooker (QSC) developed by Patel [25]. It looks like a dome-shaped transparent cover having two inner reflectors that also act as the cooking compartments. Lastly, they gave also a mathematical model for the parametric analysis of the QSC's thermal performance. The thermal efficiency of the pot is experimentally evaluated for lower temperature as well as moderate cooking temperature justification. The suggested design of solar cooker is possible to be used with glycerine as a cooking fluid with an efficiency of 9 to 92 %, and with water where efficiency ranges from 6 to 35%. Goyal and Eswaramoorthy [26] investigated the existing resources of box-type SCs that have low thermal efficiency and cannot be used for cooking during the night, which are factors that could contribute to its stability and use among many people. For better thermal performance and evening cooking practice, the removed marble pieces can be used as heat storage either as an integral part or separate heat storage. It was also advised that there should be a matte black coated aluminium sheet on the back side of the glass cover in order to reduce heat loss from on top. There were two possible configurations suggested in this study: Two cooking loads were simulated: (I) one which possessed heat storage only and no aluminium sheet; (II) and the last one containing heat storage and Aluminium sheet. Field experimentation is done, and COMSOL Multiphysics 6 was used in solving and modelling the problem. No software tool is employed to measure the increase in the level of improvement. Experimental evaluations showed that the arrangements I and II required 154–155 min and 175–176 min to cook, correspondingly. We also measured 56-62W and 48-21W, and thermal efficiencies of 25%, 79% and 31%. Some of the respondent organizations have the following employee benefit arrangements; 38% have a private health care plan, 19% have a group life assurance plan and 19% have a group personal accident insurance plan. Since the thermal conductivity of marble and the temperature availability is quite low until late evening, we analyse the heating duration to heat marble pieces of different weights using an aluminium sheet cover. The

payback period in the case of the proposed solar cooker is 1. 24 years. Such findings imply that the yearly reduction in tuberculosis incidence can be 148. Launching one solar cooker per household and if there are two people in a house, 3 kg of carbon dioxide can be eliminated on average. Banitia, et al. [27] included the conceptual development and optical evaluation of a novel solar beam-down system that can be a passive approach to indoor solar cookery, which can be beneficial and environmentally friendly. The system employs a beam-down parabolic dish concentrator which directs the solar radiation to a ground-mounted receiver module fitted with a secondary optical module comprising of a secondary reflector-light pipe assembly. The receiver module is an insulated tank that contains a receiver in direct contact with a primary heat transfer fluid. The optimal values of optical design parameters, as well as the results of the ray-trace analysis associated with them, are described. The experiment showed that the designed beam-down parabolic dish concentrator system gives out an optimal thermal energy of 10. 3 KWh per day at an average Direct Normal Irradiance (DNI) of 650 W/m^2. In addition, this study presents the theoretical design of a beam-down parabolic dish concentrating system that could be employed in a practical application on efficient and renewable solar power systems. Sivaramakrishnaiah, et al. [28] employed an LPG cooking stove for cooking; about 20 crore families use LPG for cooking in India. Currently, India imports around five lakh crores of LPG annually. Using ANSYS-CFX software, the TES system is thoroughly studied to determine its performance. A CFD analysis is done in order to find the heat transfer coefficients of the hot stream which is used to heat the bricks and the cold stream which is used to cool the heated bricks. The attained heat transfer coefficients range from 15-20 W/m^2 K of the hot fluid and 25-40 W/m^2 K of the cold fluid, with higher coefficients emanating from the increased density of air as compared to the density of the hot fluid. Interestingly, the TES system is postulated to have an average heat transfer coefficient of 20–25 W/m^2 K, thereby enabling heating and transferring of heat effectively. Hashemian and Noorpoor [29] presented a revolutionary multi-generation plant with both solar and wind energy applications. As for the present research, the idea introduced here is the cogeneration system using wind and a steam Rankine cycle. This integrated system seeks to cooling through the use of a two-cycle cooling method while heating through the use of a steam Rankine cycle heat exchanger. Moreover, the system plans to generate hydrogen with help of a proton exchange membrane electrolyzer and ammonia in a reactor. This coherent analysis examines whether there is a possibility of having a much more flexible design of the plant in question. The proposed innovative system is not only a concept to generate electricity; instead, it presents solutions for electrical (44.8 MW), heat (20.64 MW), cooling (123.9 MW), hydrogen (263.1 kg/h), and ammonia (106.48 kg/h) powers. By using thermo-economic-environmental analysis, promising performance is achieved with energetic efficiency of 83.65%, exergetic efficiency of 17.97% along with the exergo-environmental impact factor of 0.91 and total product cost rate being $1.44/s. Optimization of the parabolic trough solar collector is also significant because it accounts for the highest, 57%, of the exergy destruction rate. By comparing all the analyzed parameters of the vehicle, the optimum value of the exergo-environmental efficiency is attained at an ambient temperature of 35°C.

By assessing the current research findings, it is clear that the effect of different absorbent plate shapes on the efficiency of solar cookers with box design has not yet been comprehensively studied. This is supported by the following theoretical analysis after one run of the solar cooker with its box form as well as a porous absorber plate with some holes. An increased quantity of heat can be delivered to the air in the cooker, wherein the perforated absorber [30] contributed to it. A fair number of parties have been taking a more technical mind-set in the search for how to make solar air heaters or other solar thermal conversion gadgets more efficient.

A numerical data set courtesy of a perforated solar cooker is the main accomplishment of this study. The absorber has a porous structure and is made of perforated copper plates. It enhances the air's speedy heat transfer from the cooker due to its porous nature so that the process of cooking goes faster.

3. Simulation modelling

The GE-based simulation model is based on navigating the equations (GE) using an accurate model and numerical simulations. The fluid flow, the heat transfer, and the heat storage are done in different processes. The purpose of generating a computational model is to help work out the heating system. The heating mode is implemented in cases where you have to deal with the physical model and numerical solutions. Poiseuille's law and convective heat transfer in an unsteady state are described by ANSYS FLUENT, version 14.5 in both modes. The succeeding paragraph shows that a material can

display solid and liquid features and have the ability to hold on to and release heat by turns for a time.

3.1. Geometry

To emphasize the fact that the two stove-box types of solar cookers, which will be intended for use outside, only differ in the form of the placed plate while everything else is identical. Based on the presentation in Figure 1, the solar cooker is among the models from the subcategories that are to be numerically evaluated, and it is in a box form. The solar cookers were built using SOLIDWORKS software, which is easily attainable, and this software. Similar to the other solar box cookers, there are two wholly numbered solar cookers grid-marked, labeled '1' and '2'. The contents of the gourd are kept warm by the solid-state heat transfer that occurs as a result of the warming effect of the palm embankment inside the wooden box. Through this upper part of the glass, the only option you can be subjected to is for this part to close at an angle of 45 degrees. On the one hand, the part that involves housing is a concern for many people. The long-duration solar cooker plan slightly decreases penetration and seriously reduces factory product loss due to environmental matters. The top of the door frames is where the two glass panels can be opened simultaneously with each other and their total opening range is 2 cm. Through each of the glasses, there is a 4mm thickness of glass.

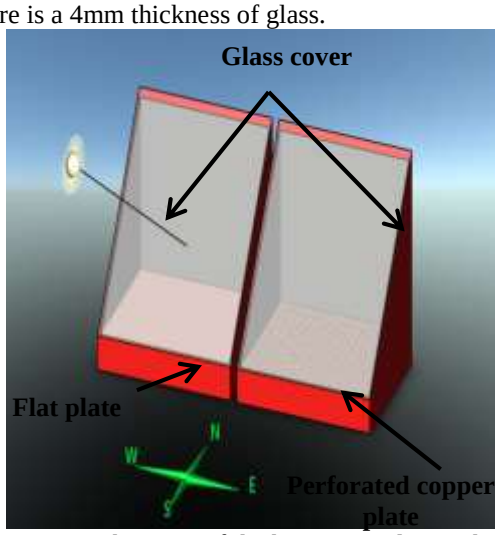

Figure 1. Schematic of the box-type solar-cookers

One early type of box solar cooker has a copper absorber plate attached to the base for efficient heat transfer. The absorber plate sheet measured 50 km in length, 60 km in breadth, and 1 mm in thickness. A second box solar cooker with dimensions of (50*60) cm^2 and a depth of 10mm was constructed using a perforated copper plate. Figure 2 shows the final cut of their application in the perforated copper plate.

Figure 2. Photograph of the perforated copper plate

In the Copper perforated plate the absorber plate, analytical testing is performed using 0, 3, 6, and 9-degree plate inclination angles against the sunlight. In addition, the data of the tests of the shaped absorber and a traditional flat plate which are positioned at similar locations are compared to identify the one that works more efficiently. A screw attaches the copper perforation plate to the wooden framework that allows it to be hung at one end (Fig.3) and lifted away from the other.

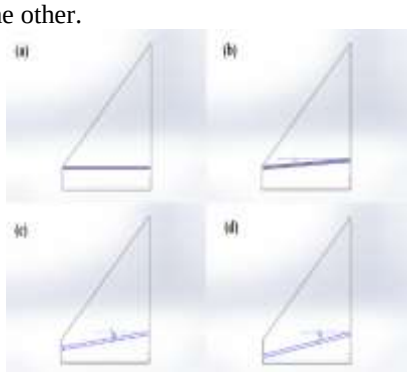

Figure 3. The schematic diagram for solar cooker with a different angle (a-0°, b-3°, c-6°, and d-9°)

3.2. Governing Equations

A mathematical model, based on firstly stated assumptions, including steady states natural convection heat transfer in the solar cooker, is developed.

I. Three-dimensional conservation equation.

II. Incompressible-flow.

III. The Boussinesq-approximation was used to establish the processes of the background density variation.

There is a generalized price indexment at his disposal based on the average temperature of every assigned attribute.

FUENTE modelling formulae concerned with fluid dynamics and heat transfer in the solar tower via free convection were mass conservation, momentum conservation, an energy equation, and a turbulence equation. Expressions such as [31] are possible with Cartesian notation:

Continuity Equation

$$\frac{\partial(\rho u)}{\partial x}+\frac{\partial(\rho v)}{\partial y}+\frac{\partial(\rho w)}{\partial z}=0 \quad (1)$$

Momentum Equation

In x-direction is:

$$\frac{\partial(\rho uu)}{\partial x}+\frac{\partial(\rho uv)}{\partial y}+\frac{\partial(\rho uw)}{\partial z} = -\frac{\partial p}{\partial x}+\frac{\partial}{\partial x}\left(\mu_{eff}\ \frac{\partial u}{\partial x}\right) + \frac{\partial}{\partial y}\left(\mu_{eff}\ \frac{\partial u}{\partial y}\right)+\frac{\partial}{\partial z}\left(\mu_{eff}\ \frac{\partial u}{\partial z}\right) + S_u \quad (2)$$

In y-direction is:

$$\frac{\partial(\rho vu)}{\partial x}+\frac{\partial(\rho vv)}{\partial y}+\frac{\partial(\rho vw)}{\partial z} = -\frac{\partial p}{\partial y}+\frac{\partial}{\partial x}\left(\mu_{eff}\ \frac{\partial v}{\partial x}\right) + \frac{\partial}{\partial y}\left(\mu_{eff}\ \frac{\partial v}{\partial y}\right)+\frac{\partial}{\partial z}\left(\mu_{eff}\ \frac{\partial v}{\partial z}\right) + S_v \quad (3)$$

In z-direction is:

$$\frac{\partial(\rho wu)}{\partial x}+\frac{\partial(\rho wv)}{\partial y}+\frac{\partial(\rho ww)}{\partial z} = -\frac{\partial p}{\partial z}+\frac{\partial}{\partial x}\left(\mu_{eff}\ \frac{\partial w}{\partial x}\right) + \frac{\partial}{\partial y}\left(\mu_{eff}\ \frac{\partial w}{\partial y}\right)+\frac{\partial}{\partial z}\left(\mu_{eff}\ \frac{\partial w}{\partial z}\right) + S_w \quad (4)$$

Energy Equation

$$\frac{\partial(\rho uT)}{\partial x}+\frac{\partial(\rho vT)}{\partial y}+\frac{\partial(\rho wT)}{\partial z} = \frac{\partial}{\partial x}\left(\Gamma_{eff}\ \frac{\partial T}{\partial x}\right) + \frac{\partial}{\partial y}\left(\Gamma\mu_{eff}\ \frac{\partial T}{\partial y}\right)+\frac{\partial}{\partial z}\left(\Gamma_{eff}\ \frac{\partial T}{\partial z}\right) + S_T \quad (5)$$

The Reynolds stresses are some kind of operators that can be represented with equations.[32]:

$$S_{u=}\ \frac{\partial}{\partial x}\left(\mu_{eff}\ \frac{\partial u}{\partial x}\right)+\frac{\partial}{\partial y}\left(\mu_{eff}\ \frac{\partial v}{\partial x}\right) + \frac{\partial}{\partial z}\left(\mu_{eff}\ \frac{\partial w}{\partial x}\right) + buoyancy \quad (6)$$

$$S_{v=}\ \frac{\partial}{\partial x}\left(\mu_{eff}\ \frac{\partial u}{\partial y}\right)+\frac{\partial}{\partial y}\left(\mu_{eff}\ \frac{\partial v}{\partial y}\right) + \frac{\partial}{\partial z}\left(\mu_{eff}\ \frac{\partial w}{\partial y}\right) + buoyancy \quad (7)$$

$$S_{w=}\ \frac{\partial}{\partial x}\left(\mu_{eff}\ \frac{\partial u}{\partial z}\right)+\frac{\partial}{\partial y}\left(\mu_{eff}\ \frac{\partial v}{\partial z}\right) + \frac{\partial}{\partial z}\left(\mu_{eff}\ \frac{\partial w}{\partial z}\right) + buoyancy \quad (8)$$

And the heat sources;

$S_{T=}\ 0$

Buoyancy (for u) = $\rho g\beta\ (T_f - T_{in})\cos(\theta)$

Buoyancy (for v) = $\rho g\beta\ (T_f - T_{in})\sin(\theta)$

θ : Angles of the chimney incline

$\Gamma_{eff} = \frac{\mu_{eff}}{\delta_{eff}} + \frac{\mu_t}{\delta_t}$

$\mu_{eff} = \mu + \mu_t$

μ_{eff} = coefficient of effective-viscosity

Γ_{eff} = coefficient of effective-diffusion

δ_{eff} = effective Prandtl-number

Turbulence Models

(k-e) Standard-Model

The k-Edison (k-) Standard model is the most common in Fluent due to its skilled applicability to every turbulent stream flow, the low computational cost, and the model's high-precision. For TKE, one can use this equation [33] to determine the turbulent kinetic-energy and the rate of dissipation. By this model, we show the way for the two-equation system resolution.

Turbulent Kinetic Energy

$$\frac{\partial}{\partial x}(\rho uK`)+\frac{\partial}{\partial y}(\rho vK`)+\frac{\partial}{\partial z}(\rho wK`) = \frac{\partial}{\partial x}\left[\Gamma_k\frac{\partial K`}{\partial x}\right]+\frac{\partial}{\partial y}\left[\Gamma_k\frac{\partial K`}{\partial y}\right] + \frac{\partial}{\partial z}\left[\Gamma_k\frac{\partial K`}{\partial z}\right]+P_k+G_k - C_D\rho\varepsilon \quad (9)$$

Where;

$\Gamma_k = \frac{\mu_{eff}}{\sigma_K}$

σ_K = Examine the empirical constant of turbulent Prandtl number when kinetic energy is used.

Dissipation Rate

$$\frac{\partial}{\partial x}(\rho u\varepsilon)+\frac{\partial}{\partial y}(\rho v\varepsilon)+\frac{\partial}{\partial z}(\rho w\varepsilon) = \frac{\partial}{\partial x}\left[\Gamma_\varepsilon\frac{\partial\varepsilon}{\partial x}\right]+\frac{\partial}{\partial y}\left[\Gamma_\varepsilon\frac{\partial\varepsilon}{\partial y}\right]+\frac{\partial}{\partial z}\left[\Gamma_\varepsilon\frac{\partial\varepsilon}{\partial z}\right]+C_{\varepsilon1}\frac{\varepsilon}{k}(P_k + C_{\varepsilon3}G_k) - C_{\varepsilon2}\rho\frac{\varepsilon^2}{k} \quad (10)$$

Where;

$\Gamma_\varepsilon = \frac{\mu_{eff}}{\sigma_\varepsilon}$

σ_ε = constant level of turbulent Prandtl number (ε). The creation of k operand by shear stress is denoted by the symbol k which is a shear stress.[34]:

$$P_k = \mu_t \left[2\left(\frac{\partial u}{\partial x}\right)^2 + 2\left(\frac{\partial v}{\partial y}\right)^2 + 2\left(\frac{\partial w}{\partial z}\right)^2 + \left(\frac{\partial u}{\partial y} + \frac{\partial v}{\partial x}\right)^2 + \left(\frac{\partial w}{\partial y} + \frac{\partial v}{\partial z}\right)^2 + \left(\frac{\partial w}{\partial x} + \frac{\partial u}{\partial z}\right)^2 \right] \quad (11)$$

The kinetic energy generation by the movement of the wave stemming from the buoyancy is the term represented by G_k, see the formula below: [35]

$$G_k = \frac{\mu_t}{\sigma_t} g\beta \frac{\partial T}{\partial y} \quad (12)$$

And the turbulent-viscosity μ_t is specified with:

$$\mu_t = \rho C_\mu \frac{k^2}{\varepsilon} \quad (13)$$

3.2.1. Mathematical Model of Porous Jump Method

The core methods of food simulation will be the enablers of this section. For this purpose, at the first step, we will investigate the subject of the issue from the angle of pressure. The presence of many materials contained in different layers gives rise to a barrier, which gives way to a drop in air pressure. Through this plate perforation, a pressure drop will be experienced as air flows through the plate because of its porous structure. Utilizing a porous media approach becomes essential due to the unfeasibility of simulating cookers utilizing computational fluid dynamics (CFD) methods. The porous media modelling can be done in different ways but the good method is to make use of the marginal hop of porous due to the elongation of the model compared to the level thickness. This has a perforated plate which is a channel for the fluid, while in each pair of two adjacent nodes, there is a porous resistance in addition to a porous jump. Based on this explanation, the porous jump method has been defined as a type of perforated filter. The first method portraying the pressure jump may be with the Darcy-Weisbach equation [36].

$$\Delta P = -\left(\frac{\mu}{\alpha} u + c\frac{1}{2}\rho u^2\right)\Delta L \quad (14)$$

In this aspect, we have the permeability coefficient (α), the viscosity of the fluid (μ), and the jump coefficient of the porous layer (c) as inputs while the thickness (ΔL) is the output. Such coefficients are attainable based only on the wind tunnel and laboratory data.

3.2.2. The Discrete-Ordinate (DO) Model

A concrete example of a discrete ordinates model is using it for radiation heat transfer. This mode shall be put in place for surface materials with semi-transparent characteristics and practically very wide uncertainty in the optical thickness. The radiative transfer equation (RTE) is given by [37] for a substance that absorbs and scatters light at a precise position r and emits light in the direction s:

$$\nabla.(I(\vec{r}, \vec{s})\vec{s}) + (a + \sigma_s) I(\vec{r}, \vec{s}) = a n^2 \frac{\sigma T^4}{\pi} + \frac{\sigma_s}{4\pi} \int_0^{4\pi} I(\vec{r}, \vec{s}') \varphi(\vec{r}, \vec{s}') d\Omega' \quad (15)$$

Assuming the following values: P(r,s) is for the solar energy amount, a is for the absorption-coefficient, n for the refractive-index, $a(\sigma)$ is for the Stefan-Boltzmann constant, and (σy) for the scattering-coefficient.

4. COMPUTATIONAL MODELING

4.1. CFD Model-Setting and Parameters

The energy and momentum equations were solved using the second-order upwind method while the pressure equations were solved using a simple standard method. All the mix of these variables mass, density, body forces, momentum, and energy were changed by the factor of 0.3, 1, 0.7, and 1, respectively. We can see in Figure 4 that models (I) and (II) needed 11500 to 12300 iterations to get the final residual value of 1800 and 2000 in the energy and continuity equations, respectively. According to this model, the velocity convergence was accomplished between 11200 and 12300 iterations at 1700 and 1300 residues in the energy equation and continuity equation.

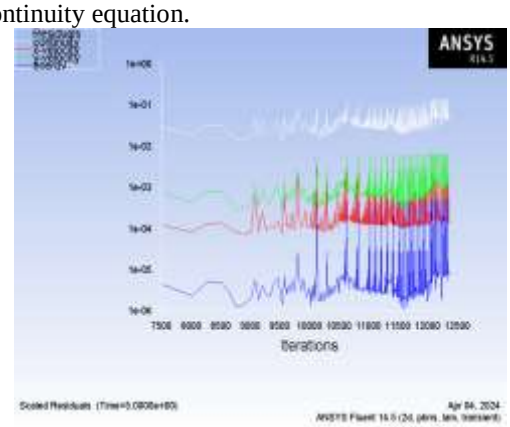

Figure 4. ANSYS FLUENT Iteration for Models

4.2. Mesh

In order to get an ANSYS FLUENT simulation that considers all the important factors and finds a

solution, the mesh quality must be high enough. To ensure that the current simulation can correctly represent the boundary layer flow and temperature gradients, enough nodes need to be strategically located next to the boundaries. However, as more nodes are added, processing becomes more resource-intensive and time-consuming yet the resolution remains the same. For both fluid-dynamics and heat-transport, a mesh that yields the essential information and is fine enough is required. As shown in Figure 5, the mesh used in this study was fine enough to explore the essential properties of fluid motion and heat transfer.

4.3. Grid Independence Test

In this case, to determine the best mesh an investigation of grid independence was conducted. The test was done on the velocity mostly in the chimney. Seven different grids were examined with 920 - 1,089 - 1,323 - 1,575 - 1,699 - 1,893 and 2,033 elements. Relative differences are quite small (less than 5 percent), to be specific, between the results of grid no. 6 and grid no. 7 for the most stringent quantities of the velocity along the solar cooker. This shows that each of the two grids in Figure 6 is almost grid independent.

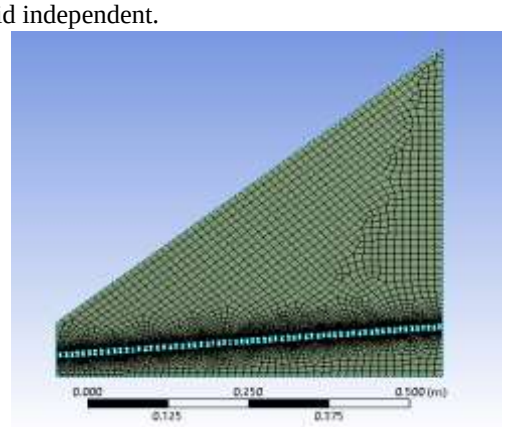

Figure 5. 3D Meshing grids of model for the perforated plate

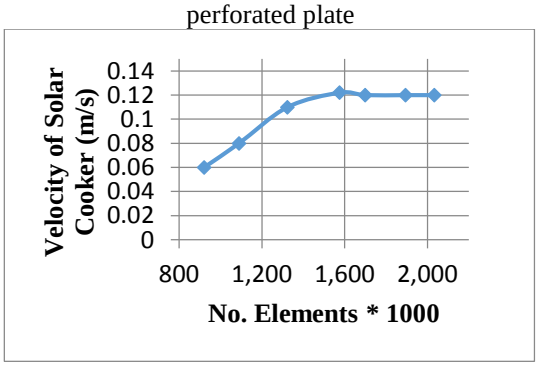

Figure 6. Avarege Air Velocity of Solar Cooker with Number of Grid Elements

4.4. The Boundary Conditions of the System

The additional boundary conditions required to augment the current study formulation are presented in Table 1 below.

Table 1. Boundary conditions of the physics models

Boundary-limit	Types	Parameters
Absorber-plate	Walls	Radiations and Mixed-Convection
Cover	Walls	Radiations and Mixed-Convection
Chamber	Walls	Heat-Flux

4.5. Properties of Materials in ANSYS

Table 2 gives an overview of the material properties of importance in the flow.

Table 2. Physical properties of materials [38]

Physical property	Absorber plate	Glass roof	Insulation	Air
Density kg/m^3	8978	1900	700	Boussi-nesq
Specific heat J/kg.K	381	837	2310	1006.43
Thermal Conductivity W/m.K	387.6	0.91	0.137	0.0242
Viscosity kg/m.s	-	-	-	1.789e-5
Refractive-index	1	1.562	1	1

4.6. Specifications of Operation Parameters

In this study, the operating pressure is 101. 325 Kpa, the reference pressure is taken as zero and the gravity effect in the case of both; vertical and inclined cooker are (X = 0 m/s^2, Y = -9.81 m/s^2, Z = 0 m/s^2). The air density was determined in this study using the Boussinesq model [39].

$$\rho \approx \rho_o - \rho_o \beta (T - T_o) \quad (16)$$

The equation of motion under the Boussinesq approximation can be expressed as:

$$\rho \frac{D}{Dt} \bar{v} = -\nabla p - \nabla \bar{\bar{\tau}} + \rho_o \bar{g} - \rho_o \bar{g} \beta (T - T_o) \quad (17)$$

The density at T_o is found as ρ_o, the density at T is described as ρ, and the expansion-coefficient is indicated as β when the input temperature is given.

5. Results

5.1. Temperature Distribution

The change of temperature contours about the perforated and flat absorber plates is shown in Figures 7-10 below which demonstrates the changes with absorber plate incline angles (0, 3, 6, and 9 degrees) at solar radiation intensities (950 W/m^2). The accumulated temperature and the perforated absorber plate of the system also grow alongside the inclining angle, reaching an overall value of 120.3 ^{o}C when the inclination angle reaches 9°. The heavier the absorber plate, the further the boundary layer spreads under the plate. Thus, thermal conduction heat turns out to be superior to convective-heat. Correspondingly, the temperatures of the absorber-plate went up as it did not transfer the heat to the surrounding air via holes in the plate.

In this case, air from the outside gets into the test cooker which is probably highly insulated. Therefore, the temperatures have remained relatively close to the ambient throughout the day. Consequently, the air in the cooker is unsuitable for people who cook; nevertheless, if we make some small corrections, we can transform it into a suitable cooking.

5.2. Density Distribution

Figures 11–14 portray the behavior of the density contours for perforated and flat absorber plates when all angles (0, 3, 6, and 9 degrees) are considered. It takes into account solar radiation intensity of about 950 W/m^2. The two density profiles: first up close to the perforated absorber plate and second far away from it are both seen decreasing while the inclination angle increases and reaches its minimum value of 0.8991 Kg/m^3 at nine degrees when the inclination angle is fully inclined. When the angle of the position of the absorber plate was increased, the boundary layer extended over the plate which had perforated holes. As a result, the conduction heat was predominant compared to the convective heat. Next, the surface temperature of the airflow plate increased because there was no heat-exchange between the air and the perforated plate.

Since the air is sucked in from the outside through an insulated test cooker, which is most likely what we share the same thing with, the dense makes is almost the same as the outside dense when the maximum solar irradiation is received. The result is a space that is unfavorable to human beings still, but with the simplest repairs, it can be changed by the wind which brings calmness.

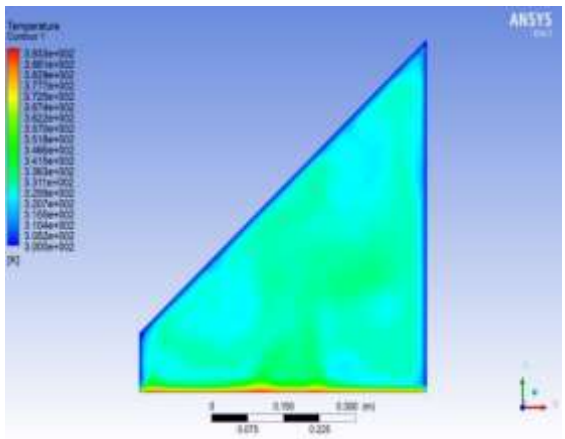

Figure 7. Temperature contour of flat absorber at 0^o

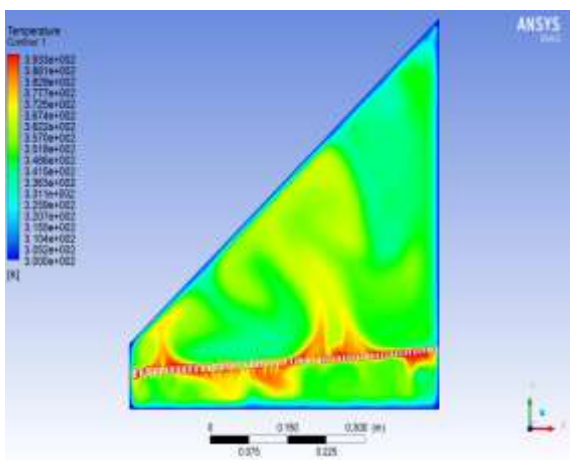

Figure 8. Temperature contour of perforated plate at 3^o

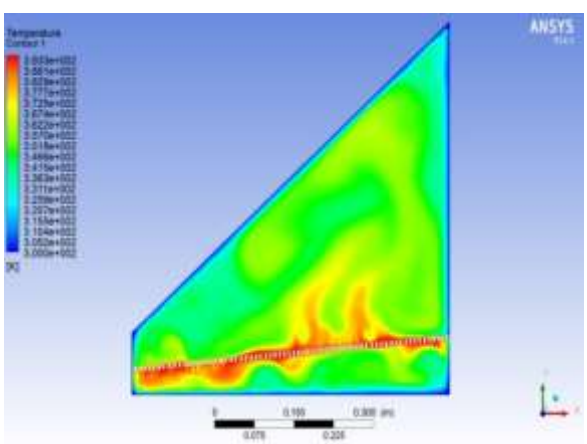

Figure 9. Temperature contour of perforated plate at 6^o

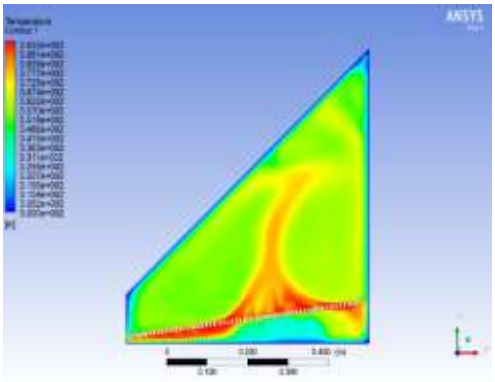

Figure 10. Temperature contour of perforated plate at 9º

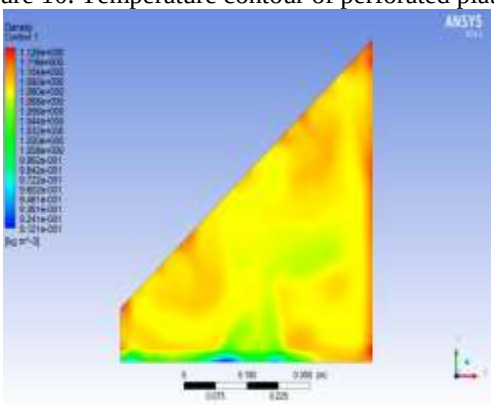

Figure 11. Density contour of flat absorber plate at 0º

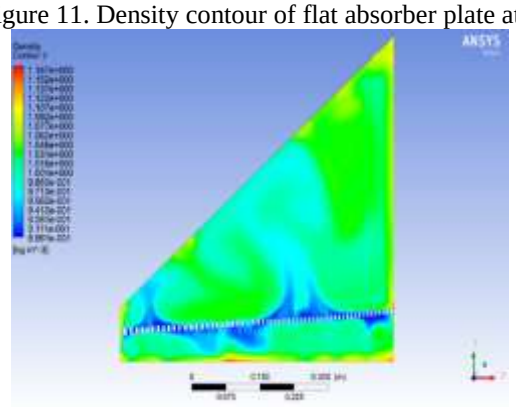

Figure 12. Density contour of perforated plate at 3º

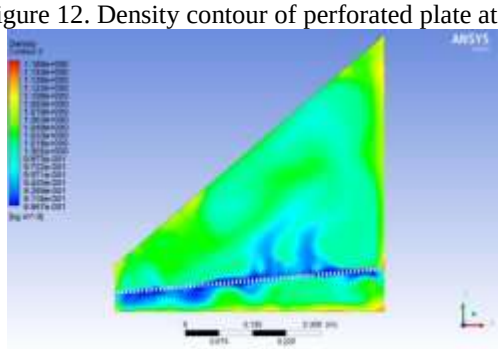

Figure 13. Density contour of perforated plate at 6º

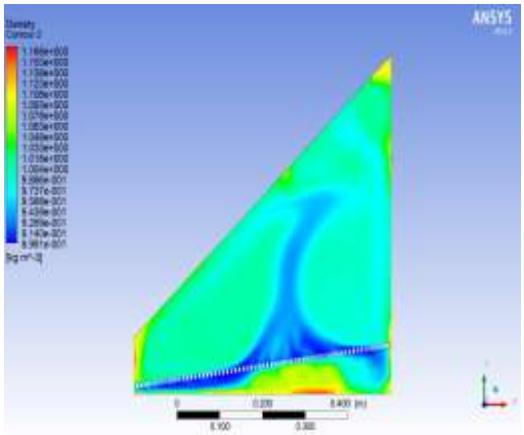

Figure 14. Density contour of perforated plate at 9º

5.3. The Standardized Cooking Power

Figure 15 shows a relation between the accumulated cooking powers (Y-axis) and the temperature differences (X-axis). It shows that the acceptable range for the equation of the cooking powers at each temperature difference is y = -16.679x + 204.18, R^2 = 0.9521. These results show that the solar cooker can be relied upon for consistently cooking food and boiling water.

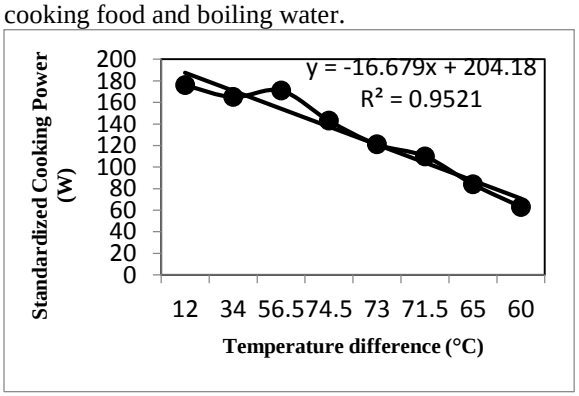

Figure 15. Relation between temperature difference and standard cooking power

5.4. Validating Results

It is clear that, adjusted to the present study and Al-Nehari et al. research [40] cooking powers are of paramount concern when it comes to assessing the competency of the quality of solar cookers to cook foods. In case of using water in the cooking fluids, the comparison of the variations of the present study and Al-Nehari et al. [40] research considering the effect of different temperature differences between the cooking fluid and the ambient air is shown in Fig. 15. Interestingly, it is also observed that present study and

Al-Nehari et al. [40] research also decreases almost linearly with temperature difference.

The R^2 of the present study and Al-Nehari et al. research [40], respectively for the regression coefficients, which implies that 0.9521 and 0.8667, respectively. These results show that values of the adjusted cooking power (P) at a temperature difference of 50 °C have been brought as the standard values because they regulate the cooker's performance as already prescribed for the international cooking power test procedure. The average value of adjusted cooking power of the present study with 50 °C temperature difference, is (176 *W*) power cooked was marginally higher than the results obtained by Al-Nehari et al. research [40] was 81 *W* and differences about 53.9%.

By observing the aspect described in Table 3, it can, however, be seen that the present solar cooker does meet with the above standard procedure.

Table 3. Comparison the present study and Al-Nehari et al. research [40] for solar cooking powers (SCP)

ΔT	Present Study	Al-Nehari et al. Research [40]	Differences %
	SCP (W)	SCP (W)	
10	176	118	32.95
20	171	104	39.18
30	166	110	33.73
40	168	92	45.24
50	176	81	53.98
60	63	55	12.70
70	112	36	67.86

6. Conclusions

The following study will present the results of experimental works that have been performed to compare two identical solar cookers, which are shaped like boxes, and all have been placed in a similar weather environment to Baghdad, Iraq. The solar cooker presented with the perforated absorber plate gives a temperature of 18, which tends to stagnate 4 times lighter than prototyping, as a flat box solar cooker with a standard absorber surface. This temperature sprouted up as the absorber plate's portion of the perforated surface was exposed to the indoor air. Further, we found out that we could successfully and significantly decrease cooking time, from 27% to 21%, when we replaced a standard flat absorber plate with a perforated one. The trend was pretty much clear as the inclination angle went up, so the mean temperatures of the perforated absorber plate also increased. It turned out that 9 degrees inclined was the optimal angle, allowing for an adequate air temperature. The comfort factor between baking times showed that the solar cooker was suitable for boiling water and cooking food. The best performance of the cooker will be achieved through the construction of a tray-shaped solar cooker with a perforated heating plate applied later. In the future, porous media will be recommended instead of perforated plates. This approach could offer enhanced efficiency and improved performance in various applications where traditional perforated plates might not be as effective.

Nomenclature

Symbol	Definition	Units
CFD	Computational Fluid Dynamic	
Conv	Convection	
DNI	Direct Normal Irradiance	
Do	Radiation Desecrate Ordinate	
GE	Governing Equations	
LPG	The liquefied petroleum gas	
PPI	Pore Per Inch	
QSC	Quonset Cooker	
Rad.	Radiation	
RNG	Re-Normalization Group	
SC	Solar Cooker	
SCP	Solar Cooking Powers	W
TES	Thermal energy storage	
η	Thermal efficiency	%
ν	Kinetic Viscosity	m^2/s
ε	Porosity, Emissivity	-
μ	Dynamic Viscosity	kg m/s
ρ	Density	kg/m^3
α_f	Thermal Diffusivity	m^2/s
α_f	Thermal Diffusivity of Fluid	m^2/s
β	Volumetric Thermal Expansion	1/K
α	Absorptivity Coefficient	-
θ	Incidence Angle	Degree
σ	Stefan – Boltzmann Constant	$W/m^2.K^4$

References

[1] Oyedepo, S. O. (2014). Towards achieving energy for sustainable development in Nigeria. *Renewable and sustainable energy reviews, 34,* 255-272. doi: https://doi.org/10.1016/j.rser.2014.03.019

[2] Bazmi, A. A., & Zahedi, G. (2011). Sustainable energy systems: Role of optimization modeling techniques in power generation and supply—A review.

Renewable and sustainable energy reviews, 15(8), 3480-3500. doi: https://doi.org/10.1016/j.rser.2011.05.003

[3] Otte, P. P. (2013). Solar cookers in developing countries—What is their key to success? *Energy Policy, 63*, 375-381. doi: https://doi.org/10.1016/j.enpol.2013.08.075

[4] Shbailat, S. J., & Nima, M. A. (2021). Possible energy saving of evaporative passive cooling using a solar chimney of metal foam porous absorber. *Energy Conversion and Management: X, 12*, 100118. doi: https://doi.org/10.1016/j.ecmx.2021.100118

[5] Mark P. McCarthy, M. J. B., Richard A. Betts. (2010). Climate change in cities due to global warming and urban effects. *Geophysical Research Letters, 37*(9). doi: https://doi.org/10.1029/2010GL042845

[6] Suhaib J Shbailat, M. N. (2024). Simulation of Effect a Variable Height of Porous Absorber on Ventilation Solar Chimney Performance. *Al-Nahrain Journal for Engineering Sciences, 26*(4), 343–350. doi: https://doi.org/10.29194/NJES.26040343

[7] Hamood, B. A. K., & Nima, M. A. (2020). Experimental Investigation of Thermal Performance of a Solar Chimney Provided with a Porous Absorber Plate. *Journal of Engineering (17264073), 26*(4). doi: https://doi.org/10.31026/j.eng.2020.04.01

[8] Bakhtiari, A. H. A. A. (2015). Efficiency Analysis of an Air Solar Flat Plate Collector in Different Convection Modes
International Journal of Green Energy, 12(9), 881-887. doi: https://doi.org/10.1080/15435075.2014.940621

[9] M. A. Al-Nimr, B. K., M. Alata. (2011). International Journal of Green Energy *A Novel Integrated Direct Absorption Self-Storage Solar Collector, 8*(6), 618-630. doi: https://doi.org/10.1080/15435075.2011.600377

[10] Ashby, M. F., & Lu, T. (2003). Metal foams: A survey. *Science in China Series B: Chemistry, 46*, 521-532. doi: https://doi.org/10.1360/02yb0203

[11] Tan, W. C., Saw, L. H., San Thiam, H., Xuan, J., Cai, Z., & Yew, M. C. (2018). Overview of porous media/metal foam application in fuel cells and solar power systems. *Renewable and sustainable energy reviews, 96*, 181-197. doi: https://doi.org/10.1016/j.rser.2018.07.032

[12] Nayak, J., Agrawal, M., Mishra, S., Sahoo, S. S., Swain, R. K., & Mishra, A. (2018). Combined heat loss analysis of trapezoidal shaped solar cooker cavity using computational approach. *Case studies in thermal engineering, 12*, 94-103. doi: https://doi.org/10.1016/j.csite.2018.03.009

[13] Ukey, A., & Katekar, V. (2019). An experimental investigation of thermal performance of an octagonal box type solar cooker. *Smart Technologies for Energy, Environment and Sustainable Development: Select Proceedings of ICSTEESD 2018*, 767-777. doi: https://doi.org/10.1007/978-981-13-6148-7_73

[14] Noman, M., Wasim, A., Ali, M., Jahanzaib, M., Hussain, S., Ali, H. M. K., & Ali, H. M. (2019). An investigation of a solar cooker with parabolic trough concentrator. *Case studies in thermal engineering, 14*, 100436. doi: https://doi.org/10.1016/j.csite.2019.100436

[15] Hashemian, N., & Noorpoor, A. (2019). Assessment and multi-criteria optimization of a solar and biomass-based multi-generation system: Thermodynamic, exergoeconomic and exergoenvironmental aspects. *Energy Conversion and Management, 195*, 788-797. doi: https://doi.org/10.1016/j.enconman.2019.05.039

[16] Engoor, G. G., Shanmugam, S., & Veerappan, A. (2020). Experimental investigation of a box-type solar cooker incorporated with Fresnel lens magnifier. *Energy Sources, Part A: Recovery, Utilization, and Environmental Effects*, 1-16. doi: https://doi.org/10.1080/15567036.2020.1826009

[17] Vengadesan, E., & Senthil, R. (2021). Experimental investigation of the thermal performance of a box type solar cooker using a finned cooking vessel. *Renewable Energy, 171*, 431-446. doi: https://doi.org/10.1016/j.renene.2021.02.130

[18] Singh, O. K. (2021). Development of a solar cooking system suitable for indoor cooking and its exergy and enviroeconomic analyses. *Solar Energy, 217*, 223-234. doi:

https://doi.org/10.1016/j.solener.2021.02.007

[19] Tawfik, M., Sagade, A. A., Palma-Behnke, R., Abd Allah, W., & Hanan, M. (2022). Performance evaluation of solar cooker with tracking type bottom reflector retrofitted with a novel design of thermal storage incorporated absorber plate. *Journal of Energy Storage, 51*, 104432. doi: https://doi.org/10.1016/j.est.2022.104432

[20] Saxena, A., Joshi, S. K., Gupta, P., Tirth, V., Suryavanshi, A., Singh, D. B., & Sethi, M. (2023). An experimental comparative analysis of the appropriateness of different sensible heat storage materials for solar cooking. *Journal of Energy Storage, 61*, 106761. doi: https://doi.org/10.1016/j.est.2023.106761

[21] Sagade, A. A., Samdarshi, S., Sagade, N. A., & Panja, P. (2021). Enabling open sun cooling method-based estimation of effective concentration factor/ratio for concentrating type solar cookers. *Solar Energy, 227*, 568-576. doi: https://doi.org/10.1016/j.solener.2021.09.035

[22] Ruivo, C. R., Apaolaza-Pagoaga, X., Coccia, G., & Carrillo-Andrés, A. (2022). Proposal of a non-linear curve for reporting the performance of solar cookers. *Renewable Energy, 191*, 110-121. doi: https://doi.org/10.1016/j.renene.2022.04.026

[23] Aquilanti, A., Tomassetti, S., Muccioli, M., & Di Nicola, G. (2023). Design and experimental characterization of a solar cooker with a prismatic cooking chamber and adjustable panel reflectors. *Renewable Energy, 202*, 405-418. doi: https://doi.org/10.1016/j.renene.2022.11.083

[24] Aquilanti, A., Tomassetti, S., Coccia, G., Muccioli, M., & Di Nicola, G. (2023). Experimental characterization and performance comparison of four prototypes of panel solar cooker for low to high sun elevations. *Journal of Cleaner Production, 390*, 136158. doi: https://doi.org/10.1016/j.jclepro.2023.136158

[25] Patel, A. (2023). Comparative thermal performance analysis of circular and triangular embossed trapezium solar cooker with and without heat storage medium. *International Journal of Science and Research (IJSR), 12*(7), 376-380. doi: http://dx.doi.org/10.21275/SR23612004356

[26] Goyal, R. K., & Eswaramoorthy, M. (2024). Theoretical and experimental analysis of box-type solar cooker with sensible heat storage. *Solar Energy, 268*, 112273. doi: https://doi.org/10.1016/j.solener.2023.112273

[27] Banitia, D., Ramachandran, S., Bhogilla, S. S., & Vijayan, P. (2024). Optical analysis and design of a novel solar beam down concentrator for indoor cooking. *Solar Compass, 12*, 100083. doi: https://doi.org/10.1016/j.solcom.2024.100083

[28] Sivaramakrishnaiah, M., Reddy, B. S. P., Subhanjeneyulu, P., Sreenivasulu, N., Veeralingam, B., Paramasivam, P., & Gurulakshmi, B. (2024). Nano-thermal energy storage system for application in solar cooker. *International Journal of Low-Carbon Technologies, 19*, 1417-1424. doi: https://doi.org/10.1093/ijlct/ctae096

[29] Hashemian, N., & Noorpoor, A. (2023). Thermo-eco-environmental Investigation of a Newly Developed Solar/wind Powered Multi-Generation Plant with Hydrogen and Ammonia Production Options. *Journal of Solar Energy Research, 8*(4), 1728-1737. doi: 10.22059/jser.2024.374028.1388

[30] Goyal, R. K. (2023). Thermo-physical properties of heat storage material required for effective heat storage and heat transfer enhancement techniques for the solar cooking applications. *Sustainable Energy Technologies and Assessments, 56*, 103078. doi: https://doi.org/10.1016/j.seta.2023.103078

[31] Getnet, M. Y., Gunjo, D. G., & Sinha, D. K. (2023). Experimental investigation of thermal storage integrated indirect solar cooker with and without reflectors. *Results in Engineering, 18*, 101022. doi: https://doi.org/10.1016/j.rineng.2023.101022

[32] Koshti, B., Dev, R., Bharti, A., & Narayan, A. (2023). Comparative performance evaluation of modified solar cookers for subtropical climate conditions. *Renewable Energy, 209*, 505-515. doi: https://doi.org/10.1016/j.renene.2023.04.021

[33] Shbailat, S. J., & Nima, M. A. (2022). Effect of absorber plate height on the performance of solar chimney utilized with porous absorber and integrated with an insulated room. *Thermal Science, 26*(6 Part A), 4775-4795. doi: https://doi.org/10.2298/TSCI211008117S

[34] Seth M. Ebersviller, J. J. J. (2022). Evaluation of performance of household solar cookers. *Solar Energy, 208*, 166-172. doi: https://doi.org/10.1016/j.solener.2020.07.056

[35] Ibrahim, O. A. A. M., Kadhim, S. A., & Ali, H. M. (2024). Enhancement the solar box cooker performance using steel fibers. *Heat Transfer, 53*(3), 1660-1684. doi: https://doi.org/10.1093/ijlct/ctae096

[36] Eyosiyas Yohannis, B., Amare Zeru, Nebiyu Bogale. (2024). Comparative CFD Analysis of Heat Transfer Enhancement in Phase Change Thermal Energy Storage with and without Fins for Solar Energy Storage. *American Journal of Bioscience and Bioinformatics, 3*(1). doi: https://doi.org/10.54536/ajbb.v3i1.2564

[37] Abdul Hussein, S. A., & Shbailat, S. J. (2023). Impact of bumpers position variation on heat exchanger performance: an experimental and predictive analysis using an artificial neural network. *Journal of Engineering and Applied Science, 70*(1), 6. doi: https://doi.org/10.1186/s44147-023-00176-x

[38] Shbailat, S. J., Rasheed, R. M., Sherza, J. S., & Ansam, A. M. (2023). Effect of inserting 10-PPI copper foam as a porous absorber on the solar cooker performance. *International Journal of Advanced Technology and Engineering Exploration, 10*(106), 1225. doi: http://dx.doi.org/10.19101/IJATEE.2023.10101244

[39] Shbailat, S. J., Rasheed, R. M., Muhi, R. J., & Mohammed, A. A. (2023). Effect of the 40-PPI copper foam layer height on the solar cooker performance. *Open Engineering, 13*(1), 20220471. doi: https://doi.org/10.1515/eng-2022-0471

[40] Al-Nehari, H. A., Mohammed, M. A., Odhah, A. A., Al-Attab, K., Mohammed, B. K., Al-Habari, A. M., & Al-Fahd, N. H. (2021). Experimental and numerical analysis of tiltable box-type solar cooker with tracking mechanism. *Renewable Energy, 180*, 954-965. doi: https://doi.org/10.1016/j.renene.2021.08.125